Journal of Electroanalytical Chemistry 782 (2016) 215–224

Contents lists available at ScienceDirect

Journal of Electroanalytical Chemistry

journal homepage: www.elsevier.com/locate/jelechem

Electrochemical immobilization of ellagic acid phytochemical on MWCNT modified glassy carbon electrode surface and its efficient hydrazine electrocatalytic activity in neutral pH☆

Annamalai Senthil Kumar [a,b,*], Ranganathan Shanmugam [a,b], Nandimalla Vishnu [a,b], K. Chandrasekara Pillai [c], Sriraghavan Kamaraj [b]

[a] Nano and Bioelectrochemistry Research Laboratory, Department of Chemistry, School of Advanced Sciences, Vellore Institute of Technology University, Vellore 632014, India
[b] Department of Chemistry, School of Advanced Sciences, Vellore Institute of Technology University, Vellore 632014, India
[c] Department of Physical Chemistry, University of Madras, Guindy Campus, Chennai 600 025, India

ARTICLE INFO

Article history:
Received 14 July 2016
Received in revised form 14 September 2016
Accepted 5 October 2016
Available online 07 October 2016

Keywords:
Ellagic acid
Phyto-chemical
Multiwalled carbon nanotube
Immobilization
Hydrazine electrocatalysis

ABSTRACT

Ellagic acid (EA) is a lactone and polyphenolic functional groups-containing phyto-chemical that has been widely used as an anti-oxidant, anti-cancer and anti-aging cosmetic agent. EA is known as a stable redox active system only in organic medium, but irreversibly oxidized with coupled chemical reactions showing ill-defined redox peaks in aqueous solutions. Interestingly, we report here that electro-oxidation of EA tethered multiwalled carbon nanotube-modified glassy carbon electrode (GCE/MWCNT@EA) showed a well-defined pair of redox peaks with a surface-confined characteristics at $E^f = 0.020$ V vs Ag/AgCl corresponding to *ortho*-quinone moiety of oxidized EA in pH 7 phosphate buffer solution (PBS). No such behavior was noticed with EA adsorbed GCE. The GCE/MWCNT@EA was characterized by cyclic voltammetery (CV) and the transfer coefficient (α) and electrode to redox surface layer electron transfer rate constant (k_s) were calculated. Physicochemical characterization of MWCNT@EA by FTIR, XRD and Raman Spectroscopy techniques revealed immobilized EA in its native form on MWCNT. Effect of various CNTs on EA electro-immobilization and the features that distinguish each other was highlighted. The GCE/MWCNT@EA showed excellent electrocatalytic activity toward N_2H_4 oxidation. The mechanism and kinetics of the catalytic reaction was investigated by CV, and the kinetic parameters ca., number of electrons in the rate determining step (n_a'), total number of electrons (n'), reaction order with respect to N_2H_4, catalyst reaction rate constant (k_{chem}) were evaluated. Finally, amperometric *i-t* and flow injection analysis for highly selective sensing of hydrazine without any interference from other biochemicals were validated.

1. Introduction

Ellagic acid (2,3,7,8-tetrahydroxy benzopyrano-5,4,3-cdebenzopyran-5,10-dione, abbreviated as EA, Scheme 1) is a polyphenolic phytochemical found widely in fruits, vegetables, seeds, and some nuts in free form or in a bound state. [1,2] Due to the presence of two pairs of neighbor hydroxyl groups in its structure, it is considered as a natural antioxidant [2] and is usually added as an ingredient in skin whitening cosmetic products. [3] Over the past few years, a number of studies on EA revealed the evidence for anti-inflammatory, anti-mutagenic and anti-carcinogenic properties [1–6]. However, most of the literature reports deal with detection of EA in various food samples using high performance-liquid chromatography [7] coupled UV detection [8] or mass spectroscopy [9], capillary electrophoresis coupled mass spectroscopy [10], voltammetric techniques [3,11–14]. Note that, EA is highly stable with well-defined redox electrochemistry in non-aqueous solvents, which allowed its use as a very good organic electrode material for rechargeable lithium batteries with high reversible capacities involving lithiation–delithiation modes at different stages of the charge–discharge process [15]. Unfortunately, electrochemical studies on redox behavior of EA on carbon surfaces in neutral pH received scant attention. For instance, in acidic and neutral conditions, EA undergoes two-stage irreversible oxidation with coupled chemical reactions showing ill-defined redox peaks on glassy carbon electrode (GCE) [16,17]. In alkaline solutions, the oxidation is still more complicated with additional formation of inactive polymerized products blocking the electrode surface at higher positive potentials [14,16,17]. Interestingly, herein, the present work we show that with a simple electrochemical-immobilization of adsorbed EA on to multi-walled carbon nanotubes (MWCNT) a highly reversible, well-defined, clean, stable, surface

☆ This work is dedicated to late Professor Ying Shih, Department of Cosmetic Science, Providence University, Taichung, 43301, Taiwan, who initiated by providing idea and sample

* Corresponding author at: Department of Chemistry, School of Advanced Sciences, Vellore Institute of Technology University, Vellore 632014, India.
E-mail address: askumarchem@yahoo.com (A.S. Kumar).

http://dx.doi.org/10.1016/j.jelechem.2016.10.010
1572-6657/

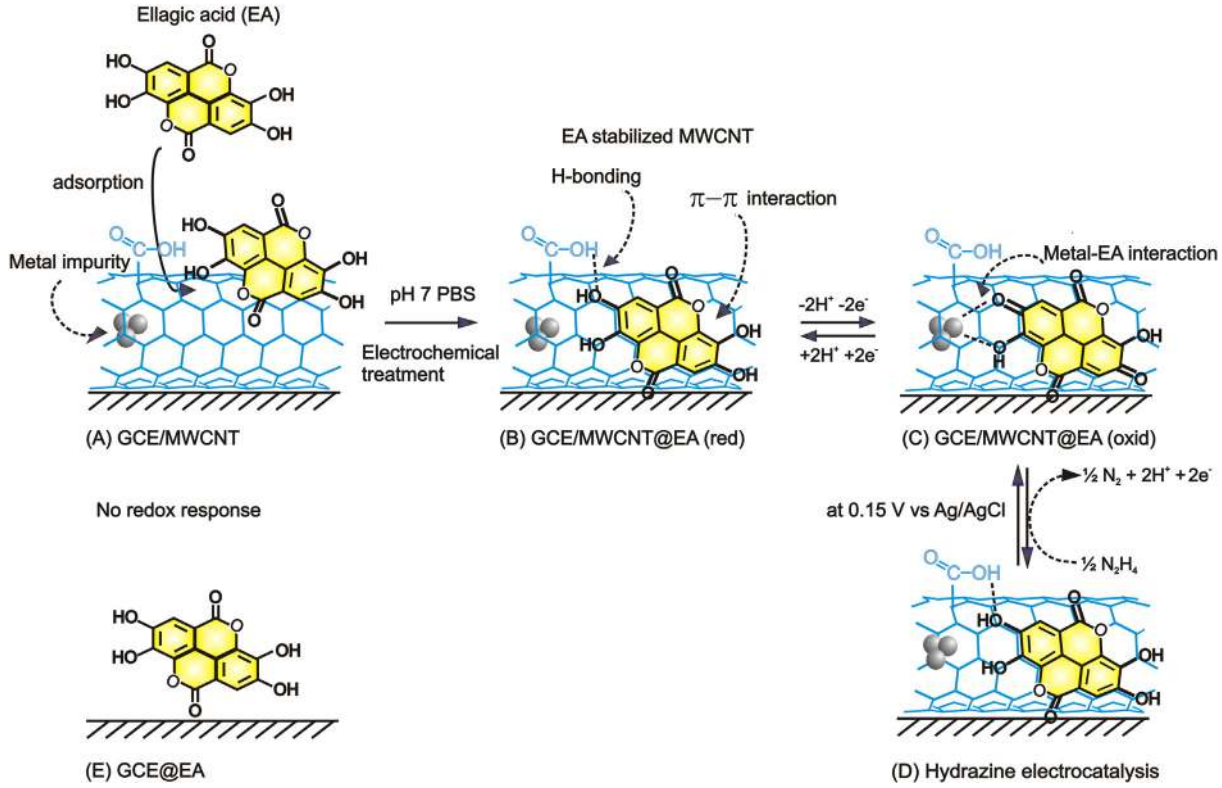

Scheme 1. Schematic illustration for adsorption (A), redox (B and C) and hydrazine electro-catalytic features of MWCNT@Ellagic acid (MWCNT@EA) (D). Illustration for the lack of immobilization and redox activity of EA on GCE surface (E).

confined pair of redox peaks is achieved in aqueous solution of pH in the range 3 to 9.

Carbon nanotubes (CNTs) are of special interest as support electrode material for immobilizing electrocatalysts and electron-mediators because of their uniquely suited properties like nano-dimension, large specific surface area, increased porosity, high electronic conductivity, amenability for introducing abundant functional groups, etc., thereby providing exciting opportunities for applications in chemical and biochemical sensors [18–20]. In this regard, our group exploited CNT for immobilization of phytochemicals such as quercetin and 8-hydroxy quinolone [21,22] as a hybrid material for electrochemical oxidation of hydrazine. A surface confined hydroquinone moiety derived from the electro-oxidation of MWCNT immobilized-phenolic quercetin yields a highly reversible pair of redox peaks, as against GCE which is electro-inactive toward quercetin oxidation, and utilized it as a stable, sensitive and selective electrochemical detector (ECD) for flow injection analysis (FIA) of hydrazine [21]. In a subsequent work, it has been shown that 8-hydroxyquinoline, which forms electro-inactive and tarry polymeric products upon electro-oxidation on GCE, produces a multi-redox active quinoline quinone intermediate strongly entrapped on MWCNT. The intermediate trapped MWCNT modified electrode shows excellent electrocatalytic behavior and amperometric current-time sensing response to hydrazine [22]. In this direction, we aimed to study the electrochemical behavior of EA on MWCNT modified GCE. Interestingly, a highly redox active surface confined oxidized form of EA immobilized in its native form without any cleavage of lactone bond has been observed upon electrochemical oxidation of EA on MWCNT in the present work (Scheme 1). Present paper deals with preparation of electrochemically-immobilized EA-MWCNT-modified GCE (GCE/MWCNT@EA), its electrochemical characterization by cyclic voltammetry (CV) in aqueous solutions of different pH 3–9 followed by MWCNT@EA material characterization by , X-ray diffraction (XRD), Fourier transform infrared (FTIR) and Raman spectroscopy. In addition to this, the electrocatalytic activity of the GCE/MWCNT@EA electrode toward hydrazine oxidation has been described along with the relevant electrode kinetic parameters evaluated. Finally, the composite electrode's promising electroanalytical performance toward selective estimation and flow injection analysis (FIA) of hydrazine in neutral pH solution has been outlined.

2. Experimental section

2.1. Reagents and materials

Ellagic acid (>95%, HPLC grade), MWCNT (~90% purity on carbon basis, size 7–15 nm × 0.5–10 μM) and SWCNT (50–70% purity on carbon basis) were purchased from Sigma-Aldrich (USA). Other chemicals used in this work were all ACS-certified reagent grade and used without further purification. Aqueous solutions were prepared using deionized and alkaline potassium permanganate distilled water. Unless otherwise stated, pH 7 phosphate buffer solution (PBS) of ionic strength, $I =$ 0.1 M was used as a supporting electrolyte in this work.

2.2. Apparatus

Voltammetric measurements were carried out with a CHI Model 660C electrochemical workstation (USA). The three-electrode system consists of chemically modified GCE as working electrode (0.0707 cm^2), Ag/AgCl as a reference electrode and platinum wire as an auxiliary electrode. XRD analysis was carried out using Bruker D8 Advanced diffractometer (Germany). FTIR analysis was carried out with a Shimadzu IR Affinity-1 spectrometer (Japan) by using KBr pellet method. Agiltron Peakseeker Pro Raman Spectrometer (USA) with a 532 nm laser probe instrument was used for Raman spectroscopic analyses. For UV/Vis spectroscopy (Jasco V-670 spectrometer, Japan) analysis, a clear ethanolic extract was used, as obtained by sonicating (3 min) the chemically modified electrode in 500 mL of ethanol followed by filtration with a membrane pore size 220 nm (Nupore). For Raman spectroscopic characterization, MWCNT@EA prepared on a disposable screen-printed

gold electrode (SPAuE), SPAuE/MWCNT@EA, was subjected to the analysis. Similarly, for FTIR and XRD, MWCNT@EA samples separated from the SPAuE/MWCNT@EA matrix using a doctor's needle (0.5 mm × 3.5 cm) were used. The FIA system consisted of Hitachi L-2130 pump delivery (Japan), a Rehodyne model 7125 sample injection valve (20 μL loop) with interconnection Teflon tube and a conventional electrochemical cell (BASi, USA) [23].

Total metal impurities (Fe, Co and Ni) in the pristine MWCNT was estimated as 5.2 wt.% by thermal gravimetric analysis [23]. Continuum source electro-thermal atomic absorption spectrometry (CS-ETAAS) studies using ZEEnit 65, Analytika Jena AG (Germany) showed 2.1 wt.% of iron impurity within the pristine MWCNT [24]. Similarly, the iron content in other carbons such f-MWCNT (0.6 wt.%), p-MWCNT (0.6 wt%) and SWCNT (0.3 wt.%) were also analysed using the CS-ETAAS [25].

2.3. Procedures

Purified MWCNT (p-MWCNT) and functionalized MWCNT (f-MWCNT) powder samples were prepared as per our previous reported procedure [21,23], where a mixture of 200 mg of 'as received' MWCNT powder + 35 mL of 6 M or 15 M HNO_3 (fuming acid) was refluxed for 12 h in a silicone oil bath at $T = 413\ (\pm 2)$ K (140 °C), filtered, washed with copious amount of DD H_2O until the pH of the filtrate became neutral, and finally dried at $T = 353\ (\pm 2)$ K (80 °C) in a vacuum oven.

Different CNTs such as 'as received' MWCNT, p-MWCNT, f-MWCNT and SWCNT were coated on GCE (GCE/MWCNT, GCE/p-MWCNT, GCE/f-MWCNT and GCE/SWCNT) by drop casting 3 μL of respective ethanolic dispersed CNT solution (2 mg/mL) on a cleaned GCE surface and allowed 5 ± 0.5 min for complete air-dry. EA was adsorbed onto CNT coated GCEs by drop casting 3 μL of a dilute EA solution (2 mg EA dissolved in 500 μL ethanol) on different GCE/CNTs, followed by 3 ± 0.5 min air-drying at room temperature. Electrochemically-immobilized EA-CNT-modified GCE (designated as GCE/CNT@EA) were prepared by repeated potential cycling of EA-adsorbed electrodes (GCE/CNT/EA) in pH 7 PBS in an optimized potential window (Supporting information, Fig. S1), −0.3 to 0.3 V vs Ag/AgCl at a scan rate (v) 50 mV s^{-1}, as illustrated in Fig.1(A). For flow injection analysis with electrochemical detection (FIA-ECD) studies, 3 μL of 0.1% Nafion-ethanolic solution coated on FIA-GCE/MWCNT@EA and dried for 5 ± 1 min at room temperature, was used as an electrochemical detector.

3. Results and discussion

3.1. Preparation of electrochemically-immobilized EA-MWCNT-modified GCE (GCE/MWCNT@EA) and electrochemical characterization

Fig. 1(A) (curve a) is a hundred continuous CV response of a EA adsorbed 'as received' MWCNT-coated GCE (GCE/MWCNT/EA), during the preparation of GCE/MWCNT@EA, in a potential window −0.3 to +0.3 V vs Ag/AgCl at $v = 50$ mV s^{-1} in pH 7 PBS. It is quite interesting that a well-defined pair of anodic and cathodic redox peaks continuously increasing with potential cycles appeared. Note that EA adsorbed GC electrode (GCE/EA) failed to show any such reversible redox peaks (Fig. 1(A) (curve b)), and only a very feeble irreversible wave-like current response was noticed agreeing well with that reported previously [17]. These observations clearly indicate the significance of the MWCNT as a matrix for the electrochemical immobilization of EA and for its high redox active electrochemical features (Scheme 1).

The GCE/MWCNT@EA film electrode after 100 cycles washed and immersed in a fresh pH 7 PBS for electrochemical characterization. Fig. 1(B) (curve a) shows that the film characteristics with respect to current and potential were retained without any alterations. The film electrode exhibited CV peaks with a formal potential, $E^f = (E_{pa} + E_{pc})/2$, −20 ± 2 mV (A1/C1) corresponding to redox reactions of the two *ortho*-hydroquinone groups of EA [14,16,17]. The film's redox response was highly stable and reproducible with no leaching of the adsorbed material over several continuous potential cycles. The surface concentration (Γ_{EA}) of the electroactive EA species responsible for A1/C1 transition was calculated with the equation [21,27]:

$$\Gamma_{EA} = Q_t / nA_{geo}F \quad (1)$$

where Q_t is the charge consumed, obtained from integrating the A1 peak area in CV under the background correction recorded at slow scan rate (5 mV s^{-1}) in pure pH 7 PBS, n, the number of electrons consumed (2 in the present case), and A_{geo} the electrode geometric area (0.0707 cm^2). Γ_{EA} was 14.81×10^{-9} mol cm^{-2}.

Effect of scan rate on the redox behavior of the GCE/MWCNT@EA in pH 7 PBS was investigated (Fig. 2(A)). A systematic increase in the redox peak currents against increase in scan rate was noticed. The ratio of cathodic-to-anodic peak currents (i_{pc}/i_{pa}) at various scan rates was almost unity. The slope value ($\partial \log\{(i_{pa})(\text{or } (i_{pc})\}/\partial \log(v)$) of double

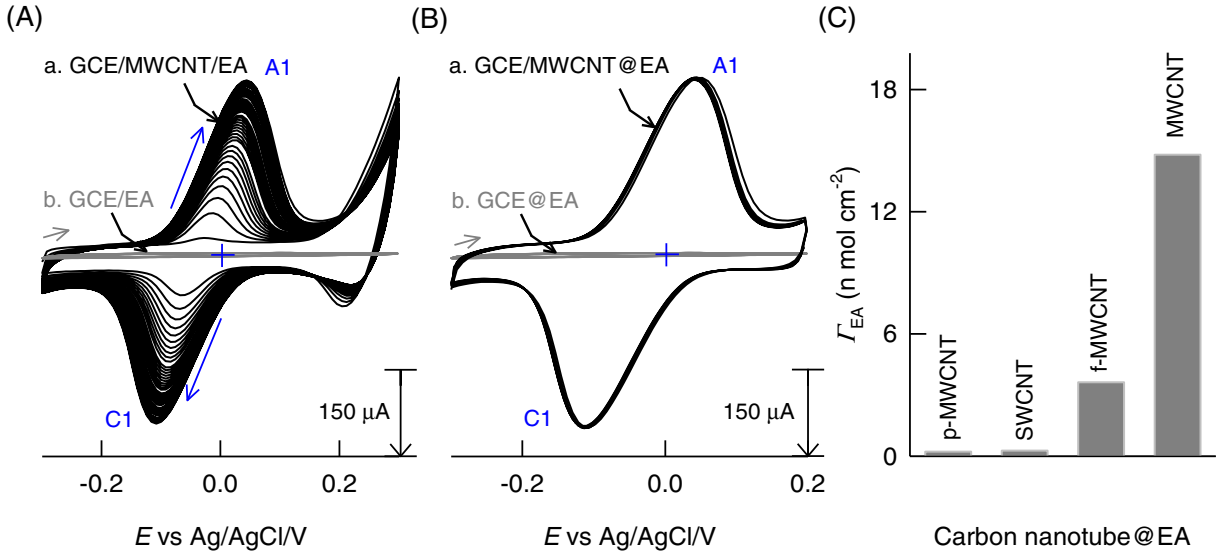

Fig. 1. (A) (a) Hundred continuous CV responses of EA adsorbed MWCNT-coated GCE, (b) CV responses of EA adsorbed GCE (pH 7 PBS, scan rate = 50 mV s^{-1}). (B): (a) Comparative CVs of GCE/MWCNT@EA, (b) GCE@EA (pH 7 PBS, scan rate = 50 mV s^{-1}). (C) Plot of Γ_{EA} vs different carbon nanotubes (CNT) in CNT@EA formation in pH 7 PBS.

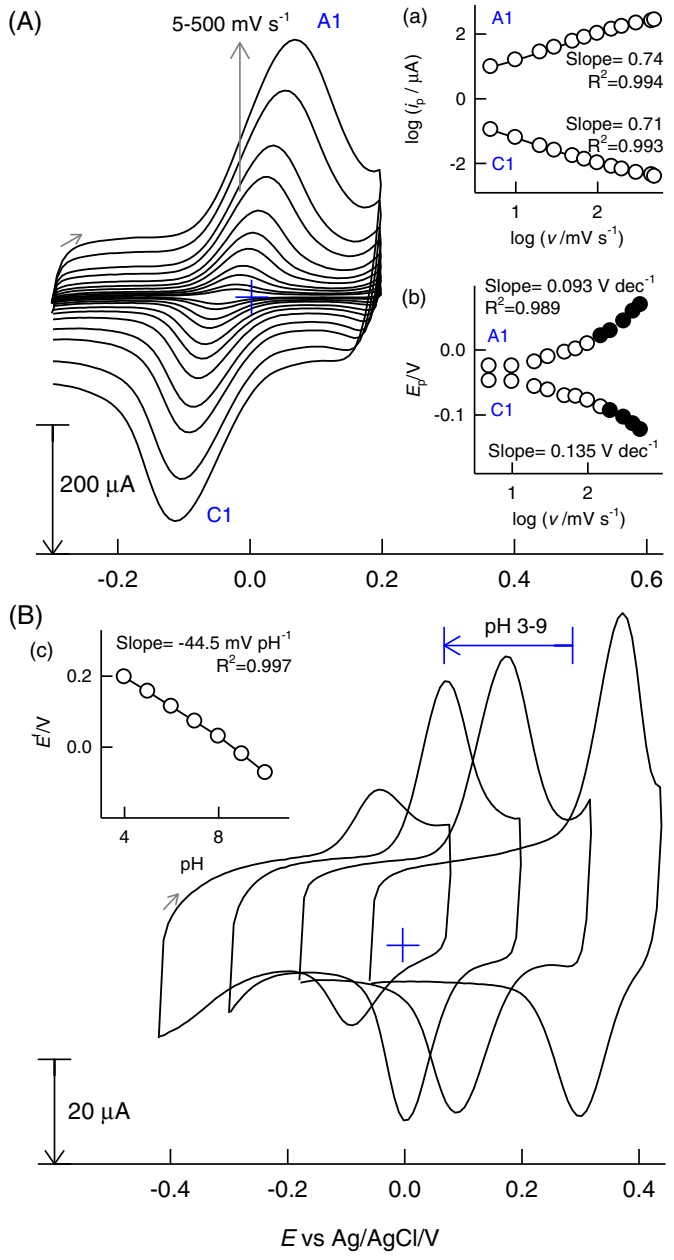

Fig. 2. Effect of scan rate in pH 7 PBS (A) and solution pH at $v = 50$ mV s^{-1} (B) on CV response of GCE/MWCNT@EA. Inset (a): log (i_p) vs log (v); inset (b): E_p vs log (v); inset (c): E^f vs pH.

logarithmic plots of i_{pa} and i_{pc} vs scan rate corresponding to A1 and C1 peaks was 0.75 (Fig. 2, inset (a)), which is in-between the ideal values of 1 and 0.5 respectively for adsorption and diffusion controlled systems, indicating operation of mixed adsorption and diffusion controlled electron-transfer processes at A1/C1. The peak potentials, E_{pa} and E_{pc} are given in Fig. 2 (inset (b)), as a function of log(v). The peak-to-peak separation potential, $\Delta E_p = E_{pa} - E_{pc}$, which was 65 ± 3 mV at $v = 50$ mV s^{-1}, increased continuously with increase in scan rate. Beyond 100 mV s^{-1}, $\Delta E_p > 90$ mV, and in this region E_{pa} and E_{pc} were linear with log(v). The surface electron transfer rate constant (k_s) and the transfer coefficient (α) were calculated from the linear E_{pa} vs log(v) plot basing on the following Laviron's equations [23,26,27] derived for $\Delta E_p > 200/n$ mV:

$$E_{pa} = E^f + [RT/(1-\alpha)n_a F \ln\{(1-\alpha)n_a F/RT][v/k_s]\} \quad (2)$$

$$\text{Slope} = [2.303RT/(1-\alpha)n_a F] = S_a \quad (3)$$

$$\text{Intercept} = E^f + S_a \log[2.303/S_a] - S_a \log[k_s] \quad (4)$$

where E^f is the formal potential of the redox couple. From the slope (0.093 V decade^{-1}), intercept (0.10 V) and $E^f = -20 \pm 2$ mV for A1/C1 (Fig. 2 (A)), α and k_s were calculated as 0.37 and 3.42 s^{-1}. The α value indicates that the quinone/hydroquinone surface redox processes were not fully reversible for the MWCNT@EA film electrode. The value of $k_s = 3.42$ s^{-1} for the EA modified MWCNT film electrode is higher than that observed for other film electrodes like MWCNT@Hb/Nf modified GCE (0.98 s^{-1}) [23] and iron hexacyanoferrate modified GCE (1.4 s^{-1}) [28] indicating better redox activity of the MWCNT@EA film.

Effect of solution pH on the redox behavior of the GCE/MWCNT@EA was examined as in Fig. 2(B). E_{pa} and E_{pc} shifted regularly to more negative values with increase in pH in the range 3–9, suggesting proton-coupled electron-transfer reactions of EA in the hybrid matrix. A plot of E^f against pH (Fig. 2, inset (c)) shows a slope value, ∂E^f/pH, −44.5 mV pH^{-1}, different from the Nerstian slope, −59 mV pH^{-1} generally observed for charge transfer processes involving equal number of protons and electrons [27]. The non-Nernstian value, −45 mV pH^{-1}, is close to −(1.5/2)(2.303RT/F) indicating involvement of non-integral values for charge and hydrogen ions. Note that non-Nernstian slope values (~−(3/2) (2.303RT/F)) have already been reported for RuO_2 electrodes either thermally prepared directly on Pt or Ti [29,30] and it has been suggested as due to the participation of non-stoichiometric inter-linked surface species arranged in net-work structures. A similar phenomenon might occur in the case of EA-immobilized-MWCNT with the CNT matrix providing the protonated oxygen functional groups for inter-linking EA redox species. However, excess of oxygen functional groups of CNT matrix found to be detrimental toward EA's electrochemical activity as shown below from electrochemical experiments with EA on different CNTs.

To examine how best the 'as received' MWCNT functions as support matrix, compared to other CNTs, toward the electrochemical activity of EA, electrochemically-immobilized EA on different CNTs viz., p-MWCNT, f-MWCNT and SWCNT were examined for EA electrochemical reaction. It was found that all the CNTs showed qualitatively similar pair of A1/C1 redox peaks with E^f around −20 mV vs Ag/AgCl; however, the peak intensity and EA surface coverage, Γ_{EA}, were significantly different. Taking Γ_{EA} as a measure of the electroactivity of immobilized EA, as displayed in the bar diagram in Fig. 1(C), one can easily find that the 'as received' MWCNT exhibited much higher surface coverage compared to all others, in the order,'as received' MWCNT (14.81 n mol cm^{-2}) > f-MWCNT (3.63 n mol cm^{-2}) > SWCNT (0.277 n mol cm^{-2}) > p-MWCNT (0.221 n mol cm^{-2}) suggesting that major electroactivity for EA was provided by 'as received' MWCNT and least activity by 'purified' MWCNT (and SWCNT). The f-MWCNT induced relatively better activity ($\Gamma_{EA} = 3.63$ nmol cm^{-2}) than the p-MWCNT and SWCNT. It is well known that CNTs contain different metal oxides, carbon materials and nano metallic components as impurities [23–25,31], and indeed, XRD and TGA identified them as Fe_2O_3, NiO, Co_2O_3, amorphous as well as graphitic carbon materials [23]. Also, the CS-ETAAS analysis indicated the contents as Fe = 21,000 ppm, Ni = 14 ppm, Co = 1.6 ppm in 'as received' MWCNT [31]. It is possible that some specific interaction like weak coordination between the metal sites of the residual metal oxides in 'as received' MWCNT and the phenolic groups [24] of EA molecule might be responsible for the highest Γ_{EA} (Fig. 1(C)) and good EA film stability (Fig. 1(B)) with this carbon material. Due to the lack of such a favorable interaction, the p-MWCNT with insufficient metal oxide impurities upon intense purification showed much weaker adsorption of EA and the lowest Γ_{EA} (0.221 n mol cm^{-2}). Similarly, as functionalization of MWCNT introduces plenty of oxy-hydroxide functional groups, such as, carboxylic (—COO—), phenolic (>C—OH), carbonyl (>C═O), hydroxyl (—OH) etc., these groups could cause repulsive interaction with the phenolic groups of EA

resulting in lower EA surface excess for f-MWCNT (3.63 n mol cm^{-2}) over 'as received' MWCNT (14.81 n mol cm^{-2}). Another reason for the diminished Γ_{EA} for the f-MWCNT may be related to its large charging background current masking the EA's redox peak response to some extent (Supporting information, Fig. S2). For the case of SWCNT, its low Γ_{EA} (0.277 n mol cm^{-2}) testifies for the difficulty in immobilizing and stabilizing the electrogenerated hydroquinone/quinone entities of the EA molecule within its single wall arrangement through π-π interaction.

It may be mentioned here that the available literature on functioning of different nanotubes, as support material for immobilizing electrocatalysts and electron-mediators, shows that only specific type of CNTs enabled surface-bound immobilization of organic molecules depending on the chemical nature of the catalysts molecules, highlighting the importance of different kinds of underlying interactions between the nanotubes and the redox mediators [21–24,31,32]. For example, the impurities-containing 'as received' MWCNT offered highest electroactivity for hemoglobin [23], benzene [24], quercetine [21], chitosan [31], etc.; but it was the purified MWCNT (p-MWCNT) that has been reported to show improved results for the quinone/hydroquinone immobilization [32]. On the other hand, for quinoline quinone [22], f-MWCNT has been found to be the best extending highest activity.

As electrochemically-immobilized EA on 'as received' MWCNT showed highest electrochemical activity, it was characterized further and applied for hydrazine sensing.

3.2. Physicochemical characterization of MWCNT@EA

In order to understand the structural features of electrochemically-immobilized EA on MWCNTs, the MWCNT@EA hybrid material was subjected to various physicochemical characterizations and the results obtained are summarized in Fig. 3. The FTIR spectra of MWCNT@EA (Fig. 3(A)(a)) showed major peaks at 3414 and 3136 cm^{-1} (νO-H stretching), 1694 cm^{-1} (νC = O stretching), 1620 cm^{-1} (νC = C, strong aromatic skeletal vibration) and 1398 and 1113 cm^{-1} (νC-O stretching). Control FTIR experiments with the individual EA and MWCNT are displayed in Fig. 3(A)(b-c). The fact that the FTIR of MWCNT@EA showed peaks similar to that by EA, but with frequency values slightly shifted within ±3 cm^{-1}, clearly indicated that EA was present in its original form in the MWCNT@EA hybrid electrode systems. Comparative XRDs of MWCNT@EA, EA and MWCNT, as given in Fig. 3(B), showed that native EA exhibited several discrete peaks. But the EA modified MWCNT electrode (MWCNT@EA) presented a broad pattern with only one peak at 25.7°, which was exactly similar to the XRD spectrum of pristine MWCNT. The absence of the characteristic peaks of EA in the XRD pattern of the MWCNT@EA composite might be due to very strong π-π interaction between EA and the impure MWCNT, manifested by immobilization and stabilization of EA within the inner walls of the nanotubes. Raman spectra of MWCNT and MWCNT@EA (Fig. 3(C)) showed specific peaks at about 1320 cm^{-1} (D band) and 1580 cm^{-1} (G band) due to the disordered graphitic structure (sp^3 bonded sites) and ordered graphitic structure (hexagonal sp^2 carbons) respectively [21,22]. The intensity ratio of the disordered band (D) to the ordered graphitic band (G) was slightly higher with MWCNT@EA ($I_D/I_G = 0.56$) than that of unmodified MWCNT ($I_D/I_G = 0.48$). The increased ratio value substantiates the existence of oxygen functional groups of immobilized EA (several sp^3 bonding) on the hybrid electrode [24], as observed above in FTIR studies. Extended characterization experiment with UV–Vis spectroscopy showed a specific and weak absorbance peak at a λ_{max} ~ 550 to 650 nm (Supporting information, Fig. S3, curve a), which may be due to a complex between Fe in 'as received' MWCNT and the phenolic groups of EA [24,33]. Overall, EA was found to be immobilized in its native form on MWCNT without any cleavage of lactone bond.

EIS is an effective method to probe the electrical properties of the materials and to monitor the changes associated with interfacial properties and thereby allowing to understand the chemical transformation and processes associated with the conductivity of the electrode surface [34]. In this study, EIS technique has been employed to elucidate comparative electron transfer behavior of the modified electrodes. All the EIS experiments were performed in an electrolyte (0.1 M KCl) solution consisting of each of 2 mM $Fe(CN)_6^{3-}$ and $Fe(CN)_6^{4-}$ at an applied potential 0.2 V vs Ag/AgCl. Fig. 4 shows the typical EIS Nyquist plot (Z′ vs Z″) for (a) bare GCE, (b) GCE/EA (c) GCE/MWCNT and (d) GCE/MWCNT@EA. The impedance data were fitted to the Randles circuit shown in the inset of Fig. 4, where R_s is electrolyte resistance, R_{ct} is charge transfer resistance, C_{dl} is double layer capacitance and Z_w is Warburg impedance. In the Randles circuit, the R_{ct} and Warburg (W) impedance can be found to be parallel to C_{dl} which results in a semicircle in the Nyquist plots. The diameter of the semicircle is equal to the R_{ct} value which is indicative of the electron transfer kinetics of the redox probe at the electrode/electrolyte interface. The Nyquist plot of bare GCE exhibits a large semicircle with an R_{ct} value of 247 Ω (Fig. 4 (curve a)), and it reduced to 170 Ω (GCE/EA; Fig. 4 (curve b)), 146 Ω (GCE/MWCNT; Fig. 4 (curve c)), and 71 Ω (GCE/MWCNT@ EA; Fig. 4 (curve d)) upon modification with EA, MWCNT and MWCNT@ EA respectively. The reduction in R_{ct} value may attribute to the increase in the electron transfer behavior of modified electrode. Hence, the hybrid film (GCE/MWCNT@EA) is the best choice for electrochemical application.

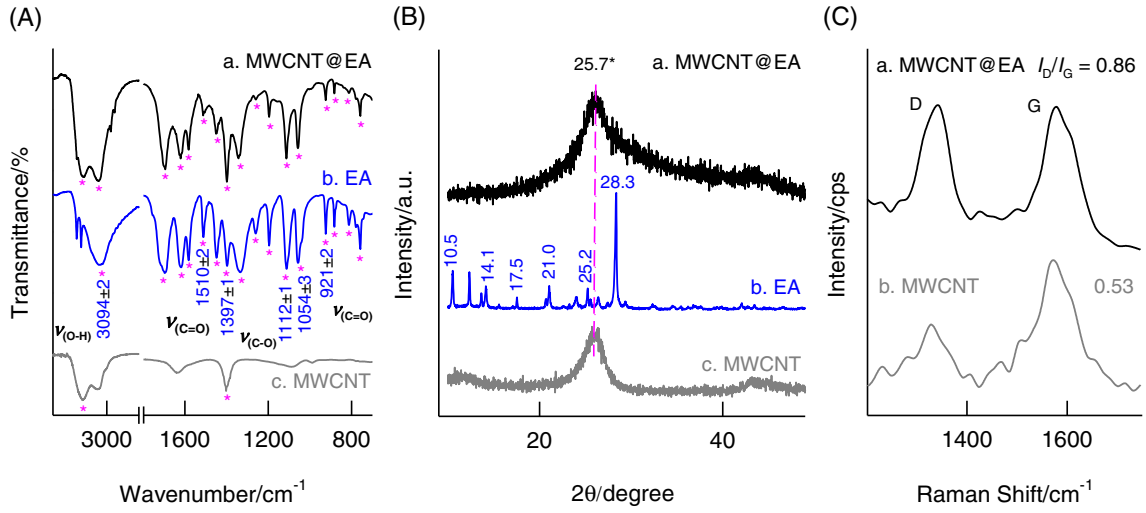

Fig. 3. FT-IR (A) and XRD (B): MWCNT (a); EA (b); MWCNT@EA (c). Raman Spectral lines (C): MWCNT (a); MWCNT@EA (b) in pH 7 PBS.

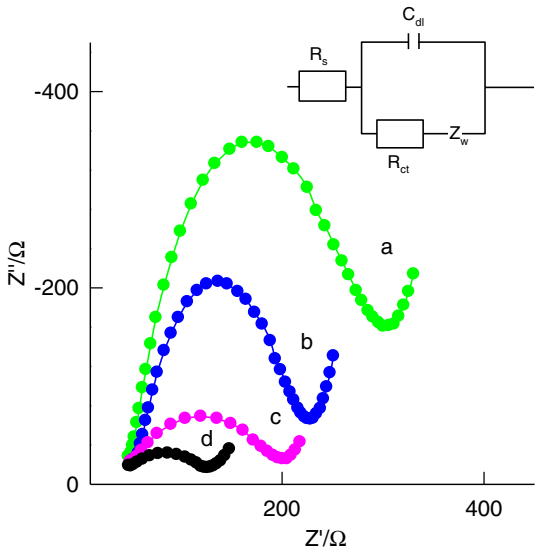

Fig. 4. EIS of GCE (a), GCE/EA (b), GCE/MWCNT (c) and GCE /MWCNT@EA with 2 mM $Fe(CN)_6^{3-}$/ $Fe(CN)_6^{4-}$ in 0.1 M KCl solution at an applied potential 0.2 V vs Ag/AgCl. Inset is Randles equivalent circuit model.

3.3. Electrocatalytic oxidation of hydrazine

To test for the electrocatalytic activity of the modified electrode toward hydrazine oxidation, CVs were traced in the absence and presence of this compound. Fig. 5(A) is the CVs of GCE/MWCNT@EA in pH 7 PBS. Upon the addition of 10 mM hydrazine, there was an increase of the anodic peak current and the cathodic peak current completely disappeared (Fig. 5(A) (curve d)) which indicates a strong catalytic effect. Note that hydrazine was not oxidized on bare MWCNT electrode (Fig. 5(A) (curve a)). Fig. 5(B) shows the dependence of the voltammetric response of the modified electrode on the hydrazine concentration. Plot of baseline corrected (catalytic) anodic peak current (i_{pa}') vs concentration of hydrazine was linear in the concentration range 0.5–9 mM with a sensitivity of 22.8 μA mM^{-1} (Fig. 5(B), inset (a)). The plot of log (i_{pa}') against log (c_{Hy}) was a straight line with slope 1.15 ± 0.04 (Fig. 5(B), inset (b)), indicating that the catalytic reaction obeys first order kinetics with respect to hydrazine in solution.

Effect of scan rate, as in Fig. 6, shows that the anodic peak current for 1 mM hydrazine on the GCE/MWCNT@EA electrode at pH 7 increased with scan rate, whereas the cathodic peak commenced to appear at scan rates beyond 30 mV s^{-1}, suggesting that the EA electrode effectively catalyses the hydrazine oxidation only at slow scan rates due to a moderate catalytic reaction rate. I_{pa}' vs $v^{1/2}$ was linear (with a slope = 259.3 μA $(V\ s^{-1})^{-1/2}$), as in Fig. 6 (inset (a)), indicating diffusion controlled electron-transfer behavior of the hydrazine oxidation on the hybrid electrode. The current function ($i_{pa}'/v^{1/2}$) for the catalytic oxidation of hydrazine decreased with scan rate (Fig. 6, inset (b)) and approached the constant value recorded for the catalyst electrode oxidation in the absence of the substrate, characteristic of an EC_{CAT} catalytic process [35]. Additionally, the peak potential for the catalytic oxidation of hydrazine shifted to more positive potentials linearly with increasing scan rate with a slope = 37.8 mV $decade^{-1}$, as in Fig. 6 (inset (c)), suggesting a kinetic limitation in the reaction between quinone/hydroquinone sites of the EA film and hydrazine.

3.3.1. Mechanism of electrocatalytic oxidation of hydrazine

The number of electrons involved in the rate determining step (n_a') and the total number of electrons involved in the hydrazine oxidation (n') are essential to elucidate the oxidation pathway of the substrate and

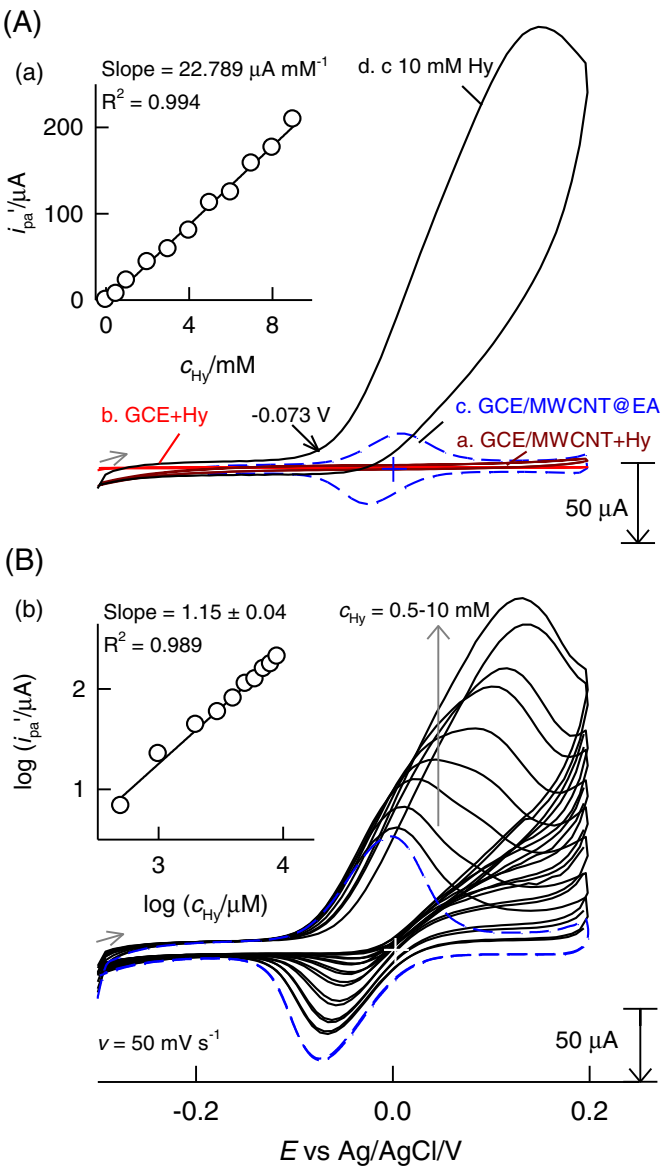

Fig. 5. (A) CV responses of GCE/MWCNT@EA without (c) and with (d) 10 mM hydrazine in pH 7 PBS at $v = 10$ mV s^{-1}. Curve (a) and (b) are the responses of GCE/MWCNT and bare GCE with 10 mM hydrazine. (B) CV responses of GCE/MWCNT@EA with various concentrations of hydrazine from 0 to 10 mM at $v = 50$ mV s^{-1}. Inset (a): i_{pa}' vs c_{Hy}; Inset (b): log (i_{pa}') vs log (c_{Hy}).

the final oxidation products. n_a' was obtained from anodic Tafel slope, $b_a = 2.303RT/(1-\alpha')n_a'F$, where α' is the transfer coefficient [36]. The necessary b_a was estimated from the slope of E_{pa} vs log(v) plot, available in Fig. 6, inset (c), which corresponds to the following Eq. (5), which is appropriate for an irreversible diffusion-controlled process [27], and also for irreversible process occurring at an electroactive thin film-coated surface [27,37–41]:

$$E_{pa} = K + (b_a/2)\log(v) \quad (5)$$

where K is a constant related to R, T, F, D_{Hy} (the diffusion coefficient of hydrazine), E^f and k_0 (the standard heterogeneous rate constant). With the slope $(\partial E_{pa}/\partial \log(v)) = 37.8$ mV $decade^{-1}$, $b_a = 2 \times 37.8 = 75.6$ mV. Alternatively, b_a was also got from Tafel plots (E vs log(i)) drawn by using the rising part of the steady-state i-E curves of 1 mM of hydrazine monitored at a slow scan rate of 5 mV s^{-1} (Fig. 7). The resulting Tafel slope ($b_a = \partial E/\partial \log(i_a)$) was 75.3 mV, close to that

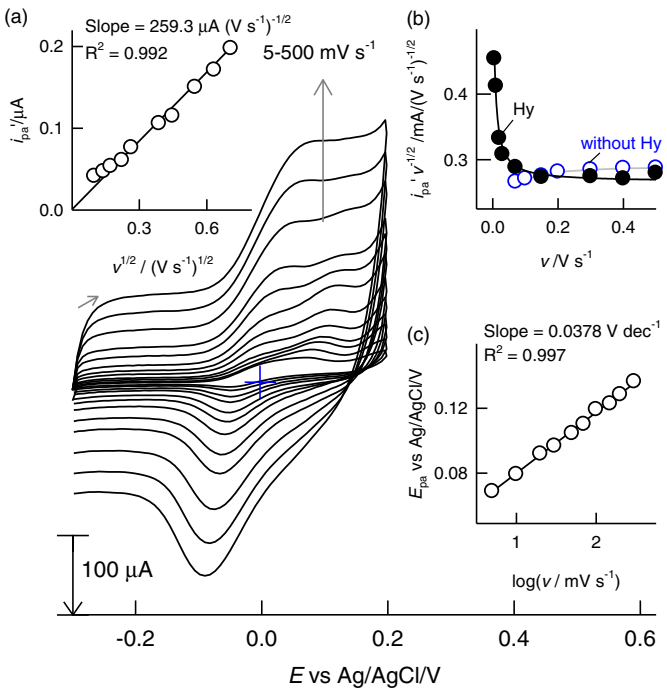

Fig. 6. CVs of GCE/MWCNT@EA electrode in presence of 1 mM hydrazine in pH 7 PBS at v = 5, 10, 20, 30, 50, 70,100, 150, 200, 400, 500 mV s^{-1}. Inset (a): i_{pa}' vs $v^{1/2}$; inset (b): $i_{pa}'/v^{1/2}$ vs v; inset (c): E_{pa} vs log (v).

from E_{pa} vs log(v) plot. From the equation $b_a = 2.303RT/(1-\alpha')n_a'F$, we can calculate $(1-\alpha')n_a' = 0.71$. If $n_a' = 1$, $\alpha' = 0.29$.

To evaluate n' value we resorted to the following equation relating i_{pa}' and $v^{1/2}$ for the totally irreversible diffusion-controlled electrode processes [27,37–41]:

$$i_{pa}' = 2.99 \times 10^5 n'[(1-\alpha')n_a']^{1/2} A_{geo} c_{Hy} D_{Hy}^{1/2} v^{1/2} \quad (6)$$

where c_{Hy} is the substrate bulk concentration. With the slope $(i_{pa}'/v^{1/2}) = 259.3 \times 10^{-6}$ A $(V\ s^{-1})^{-1/2}$ (Fig. 6 (inset (a)), $[(1-\alpha')\ n_a'] = 0.71$, $A_{geo} = 0.0707\ cm^2$, $c_{Hy} = 1.0 \times 10^{-6}$ mol cm^{-3} and $D_{Hy} = 1.4 \times 10^{-5}$ $cm^2\ s^{-1}$ [41], n' was calculated to be 3.9.

Thus, the experimental results indicate that the overall catalytic oxidation of hydrazine on GCE/MWCNT@EA electrode occurs as a four-electron process ($n' = 4$) with the rate of hydrazine oxidation controlled by the kinetics of one-electron cross-exchange reaction between the quinone sites of EA film and the substrate ($n_a = 1$) with a rate constant k_{chem}. And the catalytic oxidation obeys first-order kinetics with respect to hydrazine. However, a simple reaction mechanism accounting for all the observed results cannot be easily proposed at this stage, since the Tafel slope for the EA/hydrazine system (75 mV) is different from the conventional values 120 mV, 60 mV, 40 mV and 30 mV, which are reported for simple electrochemical reactions [36]. The occurrence of non-customary Tafel constant is an indication that the N_2H_4 oxidation on GCE/MWCNT@EA follows a complex reaction mechanism, similar to that observed earlier for Fe dissolution in HCl in presence of thiourea derivatives as corrosion inhibitors [42,43], etc. The uncommon Tafel constants observed for these systems were explained by mechanisms in which the adsorbed reaction intermediates were considered to follow Temkin adsorption isotherm [44]. A similar phenomena might occur with N_2H_4 oxidation on EA electrode in the present case. Thus, without going into details, based on the well-known 4 electron oxidation of N_2H_4 [41], the global reaction of N_2H_4 is given by

$$NH_2NH_2 + 4H_2O \rightarrow N_2 + 4\,H^+ + 4e^- \quad (7)$$

and the slow rate determining cross exchange reaction step can be written as

$$Q{-}O_2 + H_2N{-}NH_2 \xrightarrow{k_{chem}} Q{-}O(OH) + N_2H_2^{-\cdot} + H^+ + e^- \quad (8)$$

3.3.2. Kinetics of electrocatalytic oxidation of hydrazine

As per the Andrieux-Saveant model for mediation reaction at modified electrodes [45], when the electron-exchange between the electrode and the catalyst sites in the film is fast, the rate of the overall electrocatalytic reaction is controlled by diffusion of the substrate (here hydrazine) in the solution to the film surface, and three film processes, namely, substrate diffusion in the EA/MWCNT film, electron diffusion through the film and cross exchange reaction between the substrate and the quinone catalyst sites within the film, either alone or in combination [46]. When thin EA/MWCNT film and high substrate concentrations are used, the contribution of substrate and electron diffusion within the film as well as substrate diffusion in the solution to rate limiting is negligibly small and the current is determined only by the rate of the cross-exchange reaction. The corresponding catalytic rate constant, k_{chem}, can be calculated with the help of the expression for the catalytic current (i_{pa}') (Eq. 9) given by Andrieux and Saveant for a catalytic reaction in the case of slow scan rate and large k_{chem} [45].

$$i_{pa}' = 0.496 n' F A_{geo} c_s D_s^{1/2} v^{1/2} (n_a' F/RT)^{1/2} \quad (9)$$

It has been shown that in the case of fast scan rates and low k_{chem} the values of the "constant" in Eq. (9) are lower than 0.496 [47, 48]. For the present MWCNT@EA/hydrazine system with 1 mM hydrazine (Fig. 6), the average value of this coefficient was found to be 0.406. As per Fig. 1 in the paper by Andrieux and Saveant [47], where a working curve for the "constant" 0.496 was given as a function of

$$\log\left[lk_{chem}\Gamma_{EA}/\left(D_s^{1/2} v^{1/2} (n_a' F/RT)^{1/2}\right)\right] \quad (10)$$

the above function, corresponding to 0.406 value of the constant, was obtained as 0.37 (with l = 1 for a monolayer), which further allowed us to calculate k_{chem}, in the scan range 100 to 500 mV s^{-1}, to be 1.90×10^3 $mol^{-1}\ dm^3\ s^{-1}$. This value is comparable to k_{chem}, 2.2×10^3 $mol^{-1}\ dm^3\ s^{-1}$, obtained from chronoamperometry for hydrazine oxidation catalyzed by cobalt pentacyanonitrosylferrate film modified GCE [49].

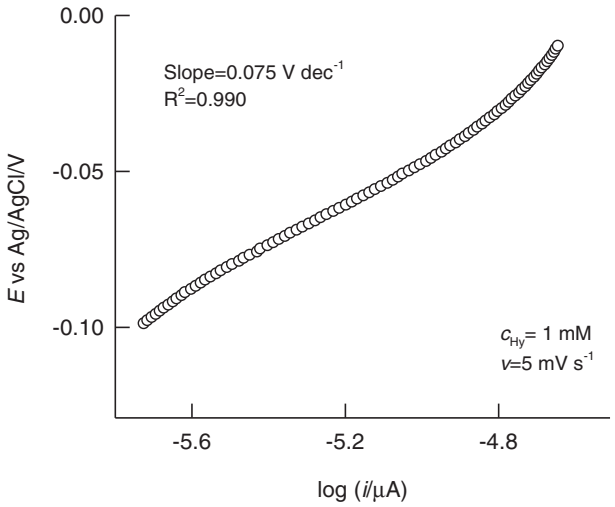

Fig. 7. Tafel plot for 1 mM hydrazine oxidation at GCE/MWCNT@EA electrode in pH 7 PBS. Rising portion of current-voltage curve recorded at v = 5 mV s^{-1} (Fig. 6) was used.

3.3.3. Amperometric and FIA estimation of hydrazine

Amperometric *i-t* detection of hydrazine on GCE/MWCNT@EA at an applied potential of 0.15 V vs Ag/AgCl was investigated as in Fig. 8(A) (curve a) and Supporting information, Fig. S4(A). Successive spikes of 25 μM hydrazine resulted in a linear increase in current signal up to 250 μM of hydrazine with a current sensitivity of 60.74 nA μM^{-1}. Control experiments with GCE/MWCNT and GCE showed low current signals toward hydrazine sensing (Fig. 8(A) (curves b & c)). Interference effects due to various environmental and biological chemicals were also examined by spiking the compounds as in Fig. 8(B) and Supporting information, Fig. S4(B). The GCE/MWCNT@EA showed remarkable tolerance to uric acid (UA), oxalic acid (OX), hydrogen peroxide (H_2O_2), cysteine (CySH), nitrite (NO_2^-), sulphate (SO_4^{2-}), nitrate (NO_3^-), magnesium (Mg^{2+}) and sodium (Na^+). These observations clearly indicate the efficient and selective electrocatalytic functioning of GCE/MWCNT@EA electrode to hydrazine detection.

Hydrazine detection was extended further by FIA-ECD experiments using a FIA-GCE/MWCNT@EA-Nf electrode consisting of 0.1% of Nafion over-layer. The Nafion used in this work was for stability purpose only. Prior to the regular FIA, inter-related hydrodynamic parameters like flow rate, H_f, and applied potential, E_{app}, were systematically optimized as $H_f = 1$ mL min^{-1} and $E_{app} = 0.3$ V vs Ag/AgCl (Supporting information, Fig. S5). Under the optimal conditions, hydrazine concentration was linear upto 1000 μM with sensitivity and regression coefficient values 10.3 nA μM^{-1} and 0.9978 respectively (Fig. 9, inset (a)). In order to check the reproducibility and stability, each hydrazine concentration was injected three times in FIA-ECD experiments. It is interesting to notice that the FIA currents were reproducible and systematically increased with increase of hydrazine concentration. Thirteen repeated injections ($n = 13$) of 5 μM hydrazine yielded a relative standard deviation (RSD) value 4.5% (Fig. 9, inset (b)). Low RSD value showed good reproducibility of the FIA-ECD and the calculated detection limit (D_L; signal-to-noise ratio = 3) was 813 nM. The calculated detection limit, sensitivity and linearity values obtained in this work are comparable with the previously reported MWCNT based amperometric sensor electrodes for hydrazine sensing and its estimation (Table 1) [21,25,32,34,50,51].

4. Conclusions

For the first time, Ellagic acid phytochemical was shown to exhibit highly redox active well-defined peaks in aqueous solution of 0.1 PBS, as against hitherto well-documented ill-defined irreversible oxidation peaks, by following a simple and elegant film preparation method, in which EA was adsorbed on to MWCNT and then electrochemically treated by potential cycling in the range −0.3 to 0.3 V vs Ag/AgCl. The electrochemically-immobilized EA-MWCNT-modified GC electrode showed stable redox peaks at $E_{1/2} = 20$ mV vs Ag/AgCl due to surface-confined *ortho*-quinone form of oxidized EA. The surface electron-transfer reaction was of mixed adsorption and diffusion controlled process. The values of electron transfer rate constant, k_s, and the transfer coefficient, α, are 3.42 s^{-1} and 0.37 respectively. Physicochemical characterization of MWCNT@ EA by FTIR, XRD and Raman Spectroscopy techniques revealed immobilized EA in its native form on MWCNT. Set

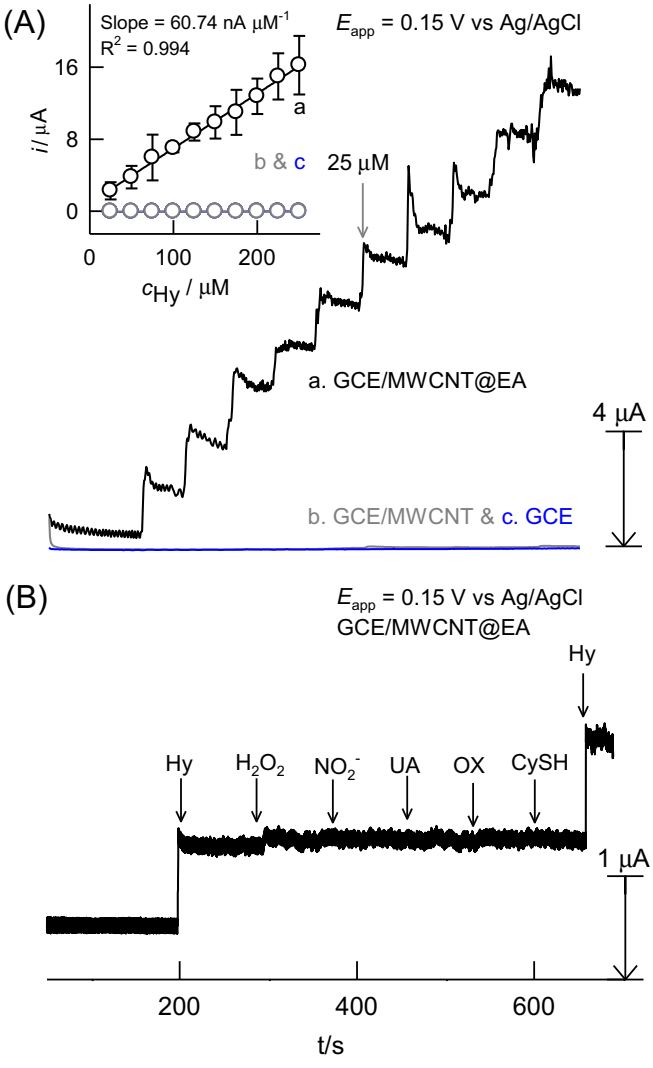

Fig. 8. Comparative amperometric *i-t* responses of (A): GCE/MWCNT@EA (a); GCE/MWCNT (b); and GCE (c) for detection of 25 μM of hydrazine. The inset is typical calibration response of: GCE/MWCNT@EA (a); GCE@EA (b); GCE (c). (B) GCE/MWCNT@EA for detection of hydrazine and other interfering biochemicals in different sequences at an applied potential of +0.15 V vs Ag/AgCl in pH 7 PBS. (Hy – Hydrazine, H_2O_2 – Hydrogen peroxide, NO_2^- - Nitrite, UA – Uric acid, OX- Oxalic acid, CySH – Cysteine).

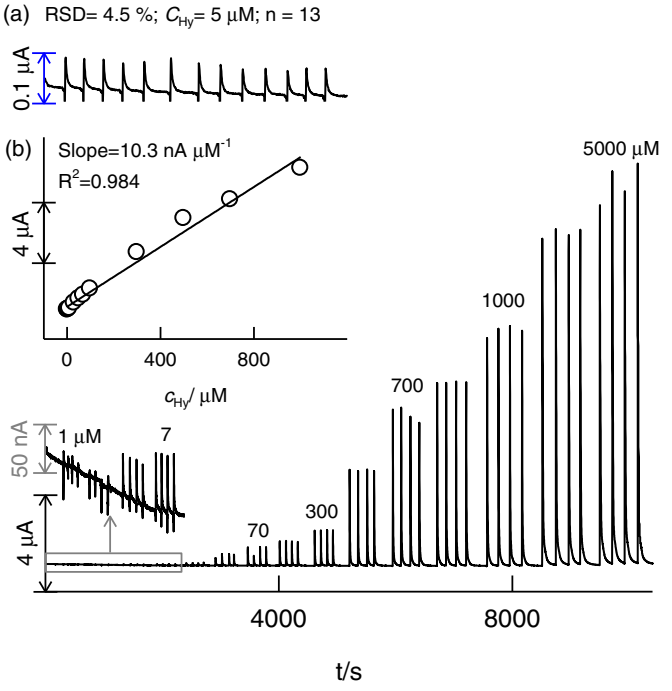

Fig. 9. FIA of GCE/MWCNT@EA/Nf for various concentrations of hydrazine. FIA parameters: $E_{app} = +0.3$ V vs Ag/AgCl; hydrodynamic flow rate (H_f) = 1 mL min^{-1}; carrier buffer solution = 0.1 M pH 7 PBS.

Table 1
Comparison of the analytical performance for the electrochemical determination of hydrazine by various chemically modified electrodes.

Modified electrode	Tech.	pH	E_{app}/V	D_L/μM	Linearity/μM	Sens. μA/μM	Ref.
1. GCE/Graphene@CoHCF	Amp *i-t*	6.5	0.66	0.069	0.25–100	0.0384	[48]
2. GCE/SWCNT@NiHCF	Amp *i-t*	7.0	0.40	0.75	20–80	0.135	[25]
3. ITO/f-MWCNT/Pd	Amp *i-t*	0.01	0.28	1.0	1–100	11.26	[34]
4. GCE/MWCNT@HQ	Amp *i-t*	7.0	0.30	78	100–1000	0.002	[32]
5. GCE/MWCNT/AuPdCu	Amp *i-t*	7.0	0.10	0.02	0.1–306	1.26	[51]
6. GCE/MWCNT@Qn	CV	7.0	0.20	–	100–3000	0.016	[21]
	Amp *i-t*			–	25–250	0.067	
	FIA			0.136	5–3000	0.008	
7. GCE/MWCNT@EA	CV	7.0		–	500–9000	0.0228	This work
	Amp *i-t*		0.15	0.86	25–250	0.06	
	FIA		0.30	0.813	1–5000	0.0103	

CoHCF = Cobalt hexacyanoferrate; NiHCF = Nickel hexacyanoferrate; ITO = Indium tin oxide; HQ = Hydroquinone; AuPdCu = Gold-Palladium-Copper; Qn = Quercetin.

of Γ_{EA} estimations with different forms of CNTs as support material revealed that specific interaction between the residual metal oxides in 'as received' MWCNT and the phenolic groups of EA molecule plays a critical role in the formation of a good, stable and highly active film with this carbon material. The electrochemically-immobilized EA on MWCNT catalyzed the electro-oxidation of N_2H_4 quite significantly through surface layer mediation. While the overall mediated catalytic N_2H_4 oxidation reaction was found to proceed with four electrons, the rate limiting slow step involved one electron, with a Tafel constant = 75 mV decade^{-1}, the order of the reaction with respect to N_2H_4 = 1, and catalyst reaction rate constant, $k_{chem} = 1.90 \times 10^3$ mol^{-1} dm^3 s^{-1}. The utility of the newly developed GCE/MWCNT@EA electrode as an electrochemical detector for N_2H_4 was verified from amperometric and FIA of hydrazine, which showed - applied potential, linear concentration range, detection limit, sensitivity, reproducibility and selectivity from among several interferents – comparable with previously reported N_2H_4 detectors.

Acknowledgments

We gratefully acknowledge the Department of Science and Technology-Science and Engineering Research Board (DST-SERB) for the financial support. We also thank DST- Technology System Development (DST-TSD) for the FIA-ECD.

Appendix A. Supplementary data

Supplementary data to this article can be found online at http://dx.doi.org/10.1016/j.jelechem.2016.10.010.

References

[1] Y.-J. Chen, N. Deng, B. Hu, Y. Wang, J.-B. He, Thin layer-based spectral and electrophoretic study of electro-oxidation of solid ellagic acid, J. Phys. Chem. B 118 (2014) 2001–2008.
[2] A. Galano, M.F. Marquez, A. Pérez-González, Ellagic acid: an unusually versatile protector against oxidative stress, Chem. Res. Toxicol. 27 (2014) 904–918.
[3] A.S. Kumar, Y.-M. Ji, S. Sornambikai, P.-Y. Chen, Y. Shih, Flow injection analysis of ellagic acid in cosmetic skin-whitening creams using a dendritic nanostructured copper-gold alloy plated screen-printed carbon electrode, Int. J. Electrochem. Sci. 6 (2011) 5344–5356.
[4] S. Sarkar, A.A. Siddiqui, S. Mazumder, R. De, S.J. Saha, C. Banerjee, M.S. Iqbal, S. Adhikari, A. Alam, S. Roy, U. Bandyopadhyay, Ellagic acid, a dietary polyphenol, inhibits tautomerase activity of human macrophage migration inhibitory factor and its pro-inflammatory responses in human peripheral blood mononuclear cells, J. Agric. Food Chem. 63 (2015) 4988–4998.
[5] P.S. Negi, G.K. Jayaprakasha, B.S. Jena, Antioxidant and antimutagenic activities of pomegranate peel extracts, Food Chem. 80 (2003) 393–397.
[6] R.W. Teel, Ellagic acid binding to DNA as a possible mechanism for its antimutagenic and anticarcinogenic action, Cancer Lett. 30 (1986) 329–336.
[7] D.V. Ratnam, V. Bhardwaj, M.N.V.R. Ravi, Simultaneous analysis of ellagic acid and coenzyme Q10 by derivative spectroscopy and HPLC, Talanta 70 (2006) 387–391.
[8] P.G. del Moral, M.J. Arin, J.A. Resines, M.T. Diez, Determination of ellagic acid in oak leaves and in sheep ruminal fluid by ion-pair RP-HPLC, J. Chromatogr. B 855 (2007) 276–281.
[9] W. Mullen, T. Yokota, M.E.J. Lean, A. Crozier, Analysis of ellagitannins and conjugates of ellagic acid and quercetin in raspberry fruits by LC–MSn, Phytochemistry 64 (2003) 617–624.
[10] J.-H. Lee, J.V. Johnson, S.T. Talcott, Identification of ellagic acid conjugates and other polyphenolics in muscadine grapes by HPLC-ESI-MS, J. Agric. Food Chem. 53 (2005) 6003–6010.
[11] J.L.R. Martins, E.A. Costa, S.H.P. Serrano, S.C. Santos, E.S. Gil, Redox behavior of the ellagitannin oenothein b and ellagic acid at a glassy carbon electrode, Int. J. Electrochem. Sci. 10 (2015) 4552–4561.
[12] S.M. Ghoreishi, M. Behpour, M. Khayatkashani, M.H. Motaghedifard, Simultaneous determination of ellagic and gallic acid in *Punica granatum*, *Myrtus communis* and itriphal formulation by an electrochemical sensor based on a carbon paste electrode modified with multi-walled carbon nanotubes, Anal. Methods 3 (2011) 636–645.
[13] M. Cuartero, J.A. Ortuno, P. Truchado, M.S. Garcia, F.A. Tomas-Barberan, M.I. Albero, Voltammetric behaviour and square-wave voltammetric determination of the potent antioxidant and anticarcinogenic agent ellagic acid in foodstuffs, Food Chem. 128 (2011) 549–554.
[14] S. Komorosky-Lovric, I. Novak, Determination of ellagic acid in strawberries, raspberries and blackberries by square-wave voltammetry, Int. J. Electrochem. Sci. 6 (2011) 4638–4647.
[15] S. Goriparti, M.N.K. Harish, S. Sampath, Ellagic acid – A novel organic electrode material for high capacity lithium ion batteries, Chem. Commun. 49 (2013) 7234–7236.
[16] H. Hotta, H. Sakamoto, S. Nagano, T. Osakai, Y. Tsujino, Unusually large numbers of electrons for the oxidation of polyphenolic antioxidants, Biochim. Biophys. Acta 1526 (2001) 159–167.
[17] A.Z. Simic, T.Z. Verbic, M.N. Sentic, M.P. Vojic, I.O. Juranic, D.D. Manojlovic, Study of ellagic acid electro-oxidation mechanism, Monatsh. Chem. 144 (2013) 121–128.
[18] M.F.L. De Volder, S.H. Tawfick, R.H. Baughman, A.J. Hart, Carbon nanotubes: present and future commercial applications, Science 339 (2013) 535–539.
[19] I. Dumitrescu, P.R. Unwin, J.V. Macpherson, Electrochemistry at carbon nanotubes: perspective and issues, Chem. Commun. 45 (2009) 6886–6901.
[20] C.B. Jacobs, M.J. Peairs, B.J. Venton, Review: carbon nanotube based electrochemical sensors for biomolecules, Anal. Chim. Acta 6620 (2010) 105–127.
[21] P. Barathi, A.S. Kumar, Quercetin tethered pristine-multiwalled carbon nanotube modified glassy carbon electrode as an efficient electrochemical detector for flow injection analysis of hydrazine in cigarette tobacco samples, Electrochim. Acta 135 (2014) 1–10.
[22] P. Swetha, K.S.S. Devi, A.S. Kumar, In-situ trapping and confining of highly redox active quinoline quinones on MWCNT modified glassy carbon electrode and its selective electrocatalytic oxidation and sensing of hydrazine, Electrochim. Acta 147 (2014) 62–72.
[23] A.S. Kumar, P. Gayathri, P. Barathi, R. Vijayaraghavan, Improved electric wiring of hemoglobin with impure-multiwalled carbon nanotube/nafion modified glassy carbon electrode and its highly selective hydrogen peroxide biosensing, J. Phys. Chem. C 116 (2012) 23692–23703.
[24] N. Vishnu, A.S. Kumar, Intrinsic iron-containing multiwalled carbon nanotubes as electro-fenton catalyst for the conversion of benzene to redox-active surface-confined quinones, ChemElectroChem 3 (2016) 986–992.
[25] N. Vishnu, A.S. Kumar, A new strategy for simple and quick estimation of redox active nickel impurity in pristine SWCNT as nickel hexacyanoferrate by electrochemical technique, Sensors Actuators B Chem. 238 (2017) 1111–1119.
[26] E. Laviron, General expression of the linear potential sweep voltammogram in the case of diffusionless electrochemical systems, J. Electroanal. Chem. 101 (1979) 19–28.
[27] A.J. Bard, L.R. Faulkner, Electrochemical Methods: Fundamentals and Applications, second ed Wiley, New York, 2009.
[28] S.M.S. Kumar, K.C. Pillai, Cetyltrimethyl ammonium bromide surfactant-assisted morphological and electrochemical changes in electrochemically prepared nanoclustered iron(III) hexacyanoferrate, J. Electroanal. Chem. 589 (2006) 167–175.
[29] L.D. Burke, O.J. Murphy, The electrochemical behaviour of RuO2-based mixed-oxide anodes in base, J. Electroanal. Chem. 109 (1980) 199–212.
[30] M.E.G. Lyons, L.D. Burke, Mechanism of oxygen reactions at porous oxide electrodes. Part 1-Oxygen evolution at RuO_2 and $RuxSn1-xO_2$ electrodes in alkaline solution under vigorous electrolysis conditions, J. Chem. Soc. Faraday Trans. 1 (83) (1987) 299–321.
[31] P. Gayathri, A.S. Kumar, An iron impurity in multiwalled carbon nanotube complexes with chitosan that biomimics the heme-peroxidase function, Chem. Eur. J. 19 (2013) 17103–17112.
[32] S. Sundaram, S.K. Annamalai, Selective immobilization of hydroquinone on carbon nanotube modified electrode via phenol electro-oxidation method and its hydrazine

electrocatalysis and *Escherichia coli* antibacterial activity, Electrochim. Acta 62 (2012) 207–217.
[33] E. Nkhili, M. Loonis, S. Mihai, H.E. Hajji, O. Dangles, Reactivity of food phenols with iron and copper ions: Binding, dioxygen activation and oxidation mechanisms, Food Funct. 5 (2014) 1186–1202.
[34] M. Rajkumar, C.P. Hong, S.M. Chen, Electrochemical synthesis of palladium nano urchins decorated multi walled carbon nanotubes for electrocatalytic oxidation of hydrazine and reduction of hydrogen peroxide, Int. J. Electrochem. Sci. 8 (2013) 5262–5274.
[35] S. Margel, F.C. Anson, Catalysis of the electroreduction of allyl chloride by cobalt 2, 2-bipyridine complexes, J. Electrochem. Soc. 125 (1978) 1232–1235.
[36] J.O. Bockris, A.K.N. Reddy, Modern Electrochemistry, Vol. 2, Plenum Press, New York, 1997.
[37] R.S. Nicholson, I. Shain, Theory of stationary electrode polarography. Single scan and cyclic methods applied to reversible, irreversible, and kinetic systems, Anal. Chem. 36 (1964) 707–723.
[38] J. Zhang, A.B.P. Lever, W.J. Pietro, Electrochemical reduction of nitrite and nitric oxide catalyzed by an iron-alizarin complexone adsorbed on a graphite electrode, Inorg. Chem. 33 (1994) 1392–1398.
[39] B. Wang, X. Cao, Anodic oxidation of hydrazine on glassy carbon modified by macrocyclic transition metal complexes: Part 1. Cobalt protoporphyrin dimethyl ester modified electrode, J. Electroanal. Chem. 309 (1991) 147–158.
[40] S. Antoniadou, A.D. Jannakdudakis, E. Theodoridou, Electrocatalytic reactions on carbon fibre electrodes modified by hemine II. Electro-oxidation of hydrazine, Synth. Met. 30 (1989) 295–304.
[41] J. Zhang, Y.-H. Tse, W.J. Pietro, A.B.P. Lever, Electrocatalytic activity of N,N′,N ,N‴-tetramethyl-tetra-3,4-pyridoporphyrazinocobalt(II) adsorbed on a graphite electrode towards the oxidation of hydrazine and hydroxylamine, J. Electroanal. Chem. 406 (1996) 203–211.
[42] K.C. Pillai, R. Narayan, The corrosion of mild steel in 0.01 M, 1 M and 3 M HCl, Corros. Sci. 22 (1982) 13–19.
[43] K.C. Pillai, R. Narayan, Anodic dissolution of mild steel in HCl solutions containing thio-ureas, R Corr. Sci. 23 (1983) 151–166.
[44] E. Gileadi, B.E. Conway, in: J.O.M.Bockris, B.E.Conway (Eds.), Modern Aspects of Electrochemistry, Vol. 4, Butterworths, London 1990, p. 70.
[45] C.P. Andrieux, J.M. Saveant, Catalysis at redox polymer coated electrodes, in: R.W. Murray (Ed.), Molecular Design of Electrode Surfaces, John Wiley & Sons, New York 1992, pp. 207–270.
[46] S.M.S. Kumar, K.C. Pillai, A kinetic study of the electrocatalytic oxidation of reduced glutathione at Prussian blue film-modified electrode using rotating-disc electrode voltammetry, Electrochim. Acta 54 (2009) 7374–7381.
[47] C.P. Andrieux, J.M. Saveant, Heterogeneous (chemically modified electrodes, polymer electrodes) vs. homogeneous catalysis of electrochemical reactions, J. Electroanal. Chem. 93 (1978) 163–168.
[48] H. Jaegfeldt, T. Kuwana, G. Johansson, Electrochemical stability of catechols with a pyrene side chain strongly adsorbed on graphite electrodes for catalytic oxidation of dihydronicotinamide adenine dinucleotide, J. Am. Chem. Soc. 105 (1983) 1805–1814.
[49] M.H. Pournaghi-Azar, R. Sabzi, Electrochemical characteristics of a cobalt pentacyanonitrosylferrate film on a modified glassy carbon electrode and its catalytic effect on the electrooxidation of hydrazine, J. Electroanal. Chem. 543 (2003) 115–125.
[50] X. Luo, J. Pan, K. Pan, Y. Yu, A. Zhong, S. Wei, J. Li, J. Shi, X. Li, An electrochemical sensor for hydrazine and nitrite based on graphene–cobalt hexacyanoferrate nanocomposite: Toward environment and food detection, J. Electroanal. Chem. 745 (2015) 80–87.
[51] F. Xu, L. Zhao, F. Zhao, L. Deng, L. Hu, B. Zeng, Electrodeposition of AuPdCu alloy nanoparticles on a multiwalled carbon nanotube coated glassy carbon electrode for the electrocatalytic oxidation and determination of hydrazine, Int. J. Electrochem. Sci. 9 (2014) 2832–2847.